Ab Initio Study of Topological Properties of 2D Crystalline Insulators

Leonardo Coscia[1*]

[1]Physics Department, University of Pisa

Abstract

Two-dimensional (2D) topological insulators (TIs) are materials that exhibit insulating behavior in their bulk while supporting conducting states at their edges. The unique electronic properties of 2D TIs arise from strong spin-orbit coupling, which leads to the formation of a band inversion and the emergence of topologically protected edge states. In this study, we employ ab initio methods based on density functional theory (DFT) to investigate the electronic structure and topological properties of two 2D crystalline insulators: phosphorene and bismuthene. We calculate the bulk band structures, density of states, and topological invariants to characterize the topological nature of these materials. We then analyze nanoribbons of these same materials, to explore their edge states and compare their properties with those predicted by the bulk topological invariants.

Introduction

The band structure of a 2D crystalline insulator is defined, due to Bloch's theorem, in the first Brillouin zone (BZ), which is a 2D torus. Eigenstates are labeled by a band index n and crystal momentum $\mathbf{k} \in \text{BZ}$. They take the form $\psi_{n\mathbf{k}}(\mathbf{r}) = e^{i\mathbf{k}\cdot\mathbf{r}} u_{n\mathbf{k}}(\mathbf{r})$, where $u_{n\mathbf{k}}(\mathbf{r})$ is a lattice-periodic function that is itself the eigenstate of the lattice-periodic Hamiltonian $H_{\mathbf{k}} = e^{-i\mathbf{k}\cdot\mathbf{r}} H e^{i\mathbf{k}\cdot\mathbf{r}}$ at energy $E_{n\mathbf{k}}$.

The band structure is therefore a map from the BZ to the Hilbert space of lattice-periodic functions. The topology of this map can be non-trivial, due to the non-trivial topology of the BZ: this is the origin of the topological properties of certain insulators [1]. The non-triviality of such a map is described by topological invariants, integers that characterize the global properties of the band structure. One such invariant is the $\mathbb{Z}_2$ invariant, which distinguishes between trivial ($\nu = 0$) and non-trivial ($\nu = 1$) topological phases in time-reversal symmetric systems [2].

An insulator is said to be a topological insulator (TI) if it has a non-trivial $\mathbb{Z}_2$ invariant $\nu = 1$. There are multiple equivalent definitions of the $\mathbb{Z}_2$ invariant. Perhaps the simplest definition, though not intuitively connected to its physical implications, is the time-reversal polarization definition [3]. In this approach, one considers the time-reversal operator Θ and defines the sewing matrix $w_{mn}(\mathbf{k}) = \langle u_{m,-\mathbf{k}} | \Theta | u_{n,\mathbf{k}} \rangle$, where m and n run over the occupied bands and $|u_{n,\mathbf{k}}\rangle$ must be continuous functions of $\mathbf{k}$. The $\mathbb{Z}_2$ invariant can then be computed as

$$(-1)^{\nu} = \prod_{i=1}^{4} \frac{\sqrt{\det[w(\Lambda_i)]}}{\text{Pf}[w(\Lambda_i)]}, \tag{1}$$

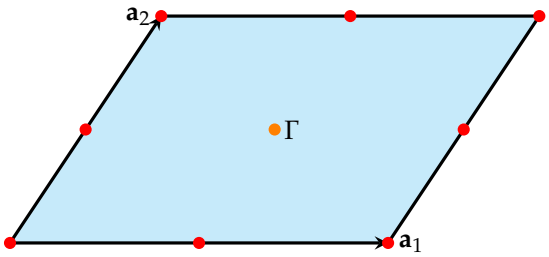

Figure 1: *BZ of a 2D material with primitive lattice vectors* $\mathbf{a}_1$ *and* $\mathbf{a}_2$*. The* Γ *point is shown in orange, the TRIM are shown in red. These points, when reflected across* Γ*, can be mapped back to themselves with a lattice translation.* Γ *is itself a TRIM. When counting TRIM, one must consider the periodicity of the BZ, which means that points on the edge count for* $1/2$*, and those in the corners count for* $1/4$*.*

where Λ_i are the four time-reversal invariant momenta[1] (TRIM) in the BZ, as seen in Fig. 1. At these points in the BZ, the sewing matrix is skew-symmetric, therefore the Pfaffian Pf is defined as the square root of the determinant in a fixed branch of the square root.

Eq. 1 is non-trivial because, when requiring the sewing matrix to be continuous in $\mathbf{k}$, we can be forced to cross the branch cut of the square root in the numerator, making its value different from the Pfaffian in the denominator.

It is known, though not proven in general, that a 2D TI must have gapless edge states at its boundaries [1]. These edge states are protected by time-reversal symmetry and are robust against non-magnetic impurities and disorder. The edge states come in pairs, called Kramers pairs, with the same energy and related by time-reversal symmetry, $\Theta |\psi_{k,\text{I}}\rangle = |\psi_{-k,\text{II}}\rangle$.

*Professor: Valentina Tozzini

Written: October 7, 2025, **Submitted:** October 10, 2025

[1] The four wavevectors which satisfy $\mathbf{k} + \mathbf{g} = -\mathbf{k}$ for some reciprocal lattice vector $\mathbf{g}$.

We say that the edge states are helical, as in their spins are locked in the same orientation relative to their momentum. States propagating in different directions on the same edge have opposite spin. This leads to a suppression of backscattering from non-magnetic impurities, as a scattering potential V that preserves time-reversal symmetry cannot couple states in a Kramers pair:

$$\begin{aligned}\langle \psi_{k,\mathrm{I}}|V|\psi_{-k,\mathrm{II}}\rangle &= \langle \psi_{-k,\mathrm{II}}|\Theta V \Theta|\psi_{k,\mathrm{I}}\rangle^* \\ &= -\langle \psi_{k,\mathrm{I}}|V|\psi_{-k,\mathrm{II}}\rangle = 0,\end{aligned}$$

where we used the anti-unitarity of Θ and the fact that $\Theta^2 = -1$ for fermions. This suppression of backscattering leads to dissipationless transport along the edges of the TI, making them promising candidates for applications in spintronics and quantum computing.

In this work, we employ ab initio methods based on density functional theory (DFT), in particular those implemented in Quantum ESPRESSO [4, 5], to investigate the electronic structure and topological properties of two 2D crystalline insulators: phosphorene and bismuthene. We calculate the bulk band structures, density of states, and topological invariants to characterize the topological nature of these materials. We then analyze nanoribbons of these same materials, to explore their edge states and compare their properties with those predicted by the bulk topological invariants.

In the first section, we present a brief overview of DFT. In the second section, we describe the computational methods and parameters used in our bulk calculations and present the results for phosphorene and bismuthene. In the third section, we describe the computational methods and parameters used in our nanoribbon calculations and present the results for phosphorene and bismuthene nanoribbons, comparing them with the bulk results.

Density Functional Theory

A system of nuclei and electrons, such as a molecule, a glass or a crystal, is described by the Hamiltonian

$$\begin{aligned}H = &-\sum_i \frac{\hbar^2\nabla_i^2}{2m_e} - \sum_I \frac{\hbar^2\nabla_I^2}{2M_I} - \sum_{i,I}\frac{Z_I e^2}{|\mathbf{r}_i - \mathbf{R}_I|} + \\ &+ \frac{1}{2}\sum_{i\neq j}\frac{e^2}{|\mathbf{r}_i - \mathbf{r}_j|} + \frac{1}{2}\sum_{I\neq J}\frac{Z_I Z_J e^2}{|\mathbf{R}_I - \mathbf{R}_J|},\end{aligned}$$

where i and j run over the electrons, I and J run over the nuclei, m_e is the electron mass, M_I and Z_I are the mass and atomic number of nucleus I, and $\mathbf{r}_i$ and $\mathbf{R}_I$ are the positions of electron i and nucleus I. The first two terms represent the kinetic energy of the electrons and nuclei, respectively. The third term represents the electron-nucleus interaction, while the fourth and fifth terms represent the electron-electron and nucleus-nucleus interactions, respectively.

Solving the Schrödinger equation for this Hamiltonian is a formidable task, due to the many-body nature of the problem. A first simplification is the Born-Oppenheimer approximation, which treats the nuclei as fixed in place, due to their mass being much larger than that of the electrons, and decouples the motion of the latter. This leads to the electronic Hamiltonian

$$H_e = -\sum_i \left[\frac{\hbar^2\nabla_i^2}{2m_e} + V_{\mathrm{ext}}(\mathbf{r}_i)\right] + \frac{1}{2}\sum_{i\neq j}\frac{e^2}{|\mathbf{r}_i - \mathbf{r}_j|},$$

where $V_{\mathrm{ext}}(\mathbf{r}_i)$ is the external potential felt by the electrons due to the nuclei, which also includes the nucleus-nucleus interaction, a constant. The electronic Schrödinger equation is then

$$H_e\Psi(\mathbf{r}_1, \mathbf{r}_2, \ldots, \mathbf{r}_N) = E\Psi(\mathbf{r}_1, \mathbf{r}_2, \ldots, \mathbf{r}_N),$$

where Ψ is the many-body wavefunction of the electrons and N is the number of electrons.

DFT is a computational method that allows us to solve the electronic Schrödinger equation by mapping the many-body problem to a single-particle problem. The key idea of DFT is that the ground-state properties of a many-electron system can be uniquely determined by its electron density $n(\mathbf{r})$, which is defined as

$$n(\mathbf{r}) = N\int |\Psi(\mathbf{r}, \mathbf{r}_2, \ldots, \mathbf{r}_N)|^2 d\mathbf{r}_2 \ldots d\mathbf{r}_N.$$

The Hohenberg-Kohn theorems [6] state that:

(i) While the external potential $V_{\mathrm{ext}}(\mathbf{r})$ uniquely determines the Hamiltonian, and therefore the ground-state wavefunction, which in turn determines the electron density, the converse is also true: the ground-state electron density $n(\mathbf{r})$ uniquely determines the external potential $V_{\mathrm{ext}}(\mathbf{r})$, up to a constant. This means that the ground-state wavefunction is a unique functional of the electron density, $\Psi = \Psi[n]$.

(ii) If one defines the energy functional

$$E[n] = F[n] + \int V_{\mathrm{ext}}(\mathbf{r})n(\mathbf{r})d\mathbf{r},$$

where $F[n] = \langle\Psi[n]|T + V_{ee}|\Psi[n]\rangle$ is a universal functional of the density, then the ground-state energy is obtained by minimizing $E[n]$ with respect to $n(\mathbf{r})$. The density that minimizes $E[n]$ is the true ground-state density of the system.

We have reduced the problem of finding the ground-state wavefunction $\Psi(\mathbf{r}_1, \mathbf{r}_2, \ldots, \mathbf{r}_N)$, which

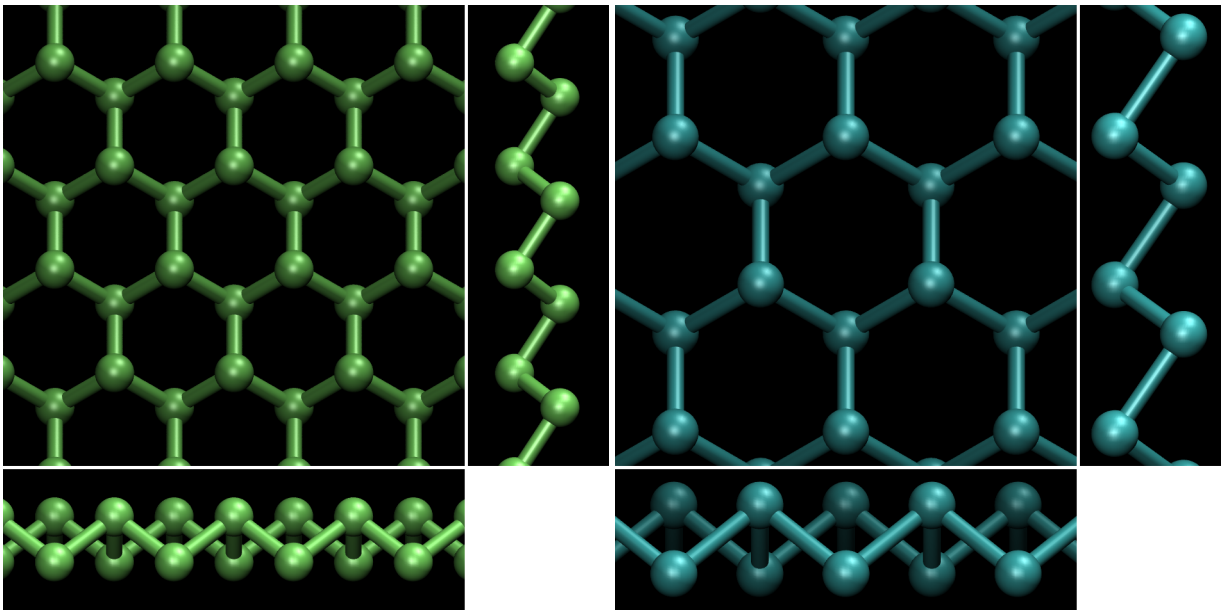

Figure 2: *Optimized structures of bulk phosphorene (left) and bismuthene (right). Images obtained in VMD [7]. The two materials have the same hexagonal lattice, with different lattice constants and out-of-plane displacements of the atoms. The lattice constants are* $a^P = 3.281$ *Å and* $a^{Bi} = 4.350$ *Å. The out-of-plane displacements are* $\Delta z^P = 1.243$ *Å and* $\Delta z^{Bi} = 1.735$ *Å.*

depends on $3N$ spatial variables, to the problem of finding the ground-state electron density $n(\mathbf{r})$, which depends on only 3 spatial variables. However, the functional $F[n]$ is not known explicitly, and approximations are needed to make DFT practical.

The most common approximation is the Kohn-Sham (KS) approach [8], which introduces a fictitious system of non-interacting electrons that has the same ground-state density as the interacting system. The KS equations are

$$\left[-\frac{\hbar^2\nabla^2}{2m_e} + V_{\text{eff}}(\mathbf{r})\right]\phi_i(\mathbf{r}) = \epsilon_i\phi_i(\mathbf{r}),$$

where $\phi_i(\mathbf{r})$ are the KS orbitals, ϵ_i are the corresponding eigenvalues, and $V_{\text{eff}}(\mathbf{r})$ is the effective potential, given by

$$V_{\text{eff}}(\mathbf{r}) = V_{\text{ext}}(\mathbf{r}) + V_H(\mathbf{r}) + V_{xc}(\mathbf{r}),$$

where $V_H(\mathbf{r})$ is the Hartree potential,

$$V_H(\mathbf{r}) = e^2\int\frac{n(\mathbf{r}')}{|\mathbf{r}-\mathbf{r}'|}d\mathbf{r}',$$

and $V_{xc}(\mathbf{r})$ is the exchange-correlation potential,

$$V_{xc}(\mathbf{r}) = \frac{\delta E_{xc}[n]}{\delta n(\mathbf{r})},$$

where $E_{xc}[n]$ is the exchange-correlation energy functional, which includes all the many-body effects not accounted for by the Hartree term. The electron density is then obtained from the KS orbitals as

$$n(\mathbf{r}) = \sum_i f_i|\phi_i(\mathbf{r})|^2,$$

where f_i are the occupation numbers of the KS orbitals. The KS equations are solved self-consistently, starting from an initial guess for the electron density, and iterating until convergence is reached. For periodic systems, such as crystals, the natural choice for the basis set is plane waves, which respect the translational symmetry of the system and are well-suited for the description of extended states.

There are many approximations for the exchange-correlation functional $E_{xc}[n]$. The simplest is the local density approximation (LDA), which assumes that the exchange-correlation energy at a point $\mathbf{r}$ depends only on the local electron density $n(\mathbf{r})$. A more accurate approximation is the generalized gradient approximation (GGA), which includes the gradient of the electron density, $\nabla n(\mathbf{r})$, in addition to the local density. A popular choice is the Perdew-Burke-Ernzerhof (PBE) functional [9], which is a type of GGA. More advanced functionals, such as meta-GGA functionals, include additional terms to improve accuracy.

Some functionals try to include part of the exact exchange energy from Hartree-Fock theory (which is lost when we assume, as we have done, that the wavefunction is a product of orbitals, without anti-symmetrization), leading to hybrid functionals. These functionals can provide better accuracy for certain systems, but are computationally more expensive.

Another important aspect of DFT calculations is the treatment of core electrons. In many cases, the core electrons do not play a significant role in the

chemical bonding and can be treated using pseudopotentials, which replace the all-electron potential with a smoother potential that reproduces the effect of the core electrons on valence electrons. This allows for a reduction in the number of plane waves needed to represent the wavefunctions, leading to significant computational savings.

There are many types of pseudopotentials, including norm-conserving pseudopotentials, ultrasoft pseudopotentials, and projector augmented-wave (PAW) potentials. The choice of pseudopotential can affect the accuracy and efficiency of the calculations.

Bulk Calculations

We performed DFT calculations for bulk phosphorene and bismuthene using Quantum ESPRESSO [4, 5], in particular the `pw.x` package. We used the PBE exchange-correlation functional [9] and norm-conserving pseudopotentials[2] [10]. The pseudopotentials used are fully relativistic, including spin-orbit coupling (SOC) effects, which are crucial for accurately describing the electronic structure of heavy elements like bismuth, especially when investigating topological properties.

All calculations[3] are done on a single unit cell, with non-collinear SOC and without constraints on magnetization, which, in Quantum ESPRESSO, means setting an initial non-zero value for the magnetization. A vacuum of 5 times the lattice constant is added in the out-of-plane direction to avoid interactions between periodic images.

The scf and vc-relax[4] calculations are done with a $12 \times 12 \times 1$ Monkhorst-Pack [11] k-point grid, a plane wave cutoff of 50 Ry and a density cutoff of 200 Ry. The nscf calculation is done with a $32 \times 32 \times 1$ Monkhorst-Pack k-point grid, a plane wave cutoff of 75 Ry and a density cutoff of 300 Ry. The same cutoffs are used in the band calculation.

The scf energy convergence threshold is set to 10^{-8} Ry. The vc-relax total energy convergence threshold is set to 10^{-5} Ry and the force convergence threshold is set to 10^{-4} Ry/Å.

The initial structures of phosphorene and bismuthene, taken from the Materials Cloud database [12], were originally obtained through computational exfoliation and relaxation of their three-dimensional bulk counterparts [13]. After a first scf calculation to test convergence, a vc-relax structure and cell optimization was run to obtain the structures of Fig. 2. We can see that the two crystals have the same hexagonal lattice, the only differences being the lattice constant

$$a^{\mathrm{P}} = 3.281\,\text{Å}, \qquad a^{\mathrm{Bi}} = 4.350\,\text{Å},$$

and the out of plane displacement of the atoms

$$\Delta z^{\mathrm{P}} = 1.243\,\text{Å}, \qquad \Delta z^{\mathrm{Bi}} = 1.735\,\text{Å}.$$

The ratios of out of plane displacements to lattice constant for the two materials are:

$$\Delta z^{\mathrm{P}}/a^{\mathrm{P}} = 0.379, \qquad \Delta z^{\mathrm{Bi}}/a^{\mathrm{Bi}} = 0.399.$$

In both structures, the distance between atoms in the unit cell remains $a/\sqrt{3}$. In other words, the planar structure remains a perfectly symmetric honeycomb lattice.

This is the reason the materials were chosen: despite being very similar structurally[5], we will see that the higher mass of bismuth makes more relevant the relativistic effects that can lead to topological non-triviality.

The optimized structure was then used to perform a more precise nscf calculation, the results of which were used to compute the density of states using `dos.x`. An nscf band calculation was also done along high-symmetry directions of the BZ. The bands were untangled with `bands.x`, so that they could be plotted along with the density of states. The results are

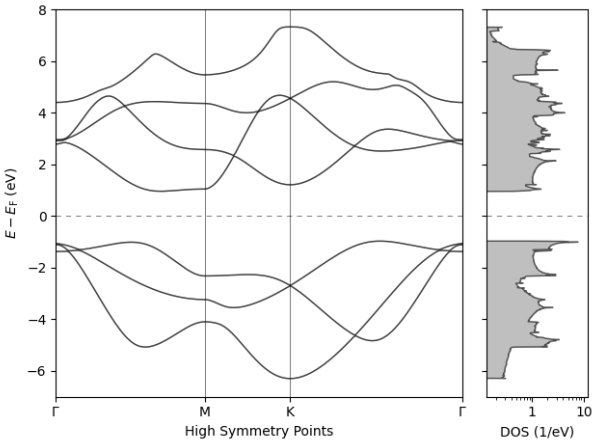

Figure 3: *Computed density of states (on the right) and band structure along high-symmetry directions in the BZ (on the left) for bulk phosphorene. The energies are given with respect to the Fermi energy, which lies in the middle of the gap. This is because the absolute energy is defined up to a constant, and different pseudopotentials are incompatible when it comes to this shift in energy. The gap is* $E_G^P = 1.9319\,\text{eV}$ *and the direct gap is* $E_{DG}^P = 2.1219\,\text{eV}$.

[2] Unfortunately, there is no citation available for the Bismuth pseudopotential. Both pseudopotential files can be found at https://github.com/coscialeo/num_meth.git.

[3] Input files are available at https://github.com/coscialeo/num_meth.git.

[4] Structure and cell optimization.

[5] The planar projections are identical up to a rescaling, while in the out of plane direction, after the rescaling, they differ by a factor of 5%.

shown in Figs. 3 and 4. We can see that both materials are insulators, as expected. The computed band gaps[6] are:

$$E_G^{\mathrm{P}} = 1.9319\,\mathrm{eV}, \qquad E_G^{\mathrm{Bi}} = 0.5371\,\mathrm{eV},$$

while the direct gaps are

$$E_{DG}^{\mathrm{P}} = 2.1219\,\mathrm{eV}, \qquad E_{DG}^{\mathrm{Bi}} = 0.6010\,\mathrm{eV}.$$

To compute the $\mathbb{Z}_2$ invariant, we used the `pw2wannier90.x` module to translate the computed orbitals into the input files for Wannier90 [15] to obtain the maximally-localized Wannier functions. The output of this calculation is then fed to WannierTools [14], which is able to compute topological invariants and other geometric/topological properties of the band structure of the tight-binding Hamiltonian obtained through Wannier90.

We use WannierTools to do a Wilson loop calculation of the $\mathbb{Z}_2$ invariant [16]. The Wilson loop is defined as the path-ordered exponential of the non-Abelian Berry connection along a closed loop C in the BZ:

$$\mathcal{W}(C) = \mathcal{P} \exp\left(i \oint_C \mathbf{A}(\mathbf{k}) \cdot d\mathbf{k} \right),$$

where $\mathbf{A}(\mathbf{k})$ is the Berry connection, defined as

$$\mathbf{A}_{mn}(\mathbf{k}) = i \langle u_{m\mathbf{k}} | \nabla_{\mathbf{k}} | u_{n\mathbf{k}} \rangle .$$

Given the toroidal topology of the BZ, we can define loops at fixed k_x that wind around the BZ in the k_y direction. We then have a family of Wilson loops $\mathcal{W}(k_x)$. The eigenvalues of the Wilson loop operator can be written as $e^{i\theta_n(k_x)}$, where $\theta_n(k_x)$ are the so-called Wannier charge centers (WCCs). The $\mathbb{Z}_2$ invariant can then be computed by tracking the evolution of the WCCs as k_x varies from 0 to π/a. If an odd number of WCCs cross a reference line during this evolution, the system is in a topological phase ($\nu = 1$); if an even number of crossings occur, the system is in a trivial phase ($\nu = 0$).

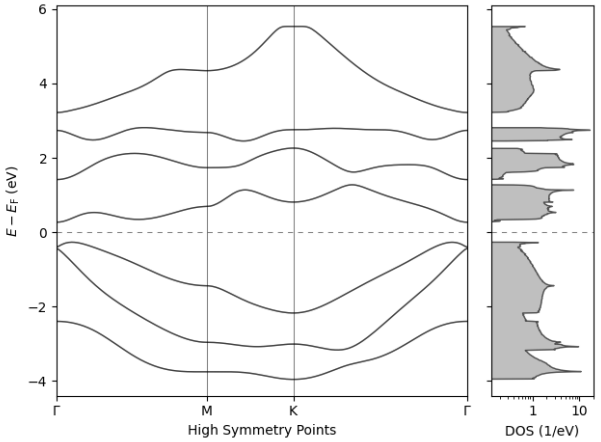

Figure 4: *Computed density of states (on the right) and band structure along high-symmetry directions in the BZ (on the left) for bulk bismuthene. The energies are given with respect to the Fermi energy, which lies in the middle of the gap. This is because the absolute energy is defined up to a constant, and different pseudopotentials are incompatible when it comes to this shift in energy. The gap is $E_G^{Bi} = 0.5371\,\mathrm{eV}$ and the direct gap is $E_{DG}^{Bi} = 0.6010\,\mathrm{eV}$.*

[6] It is important to remember that DFT with LDA and GGA functionals systematically underestimates band gaps.

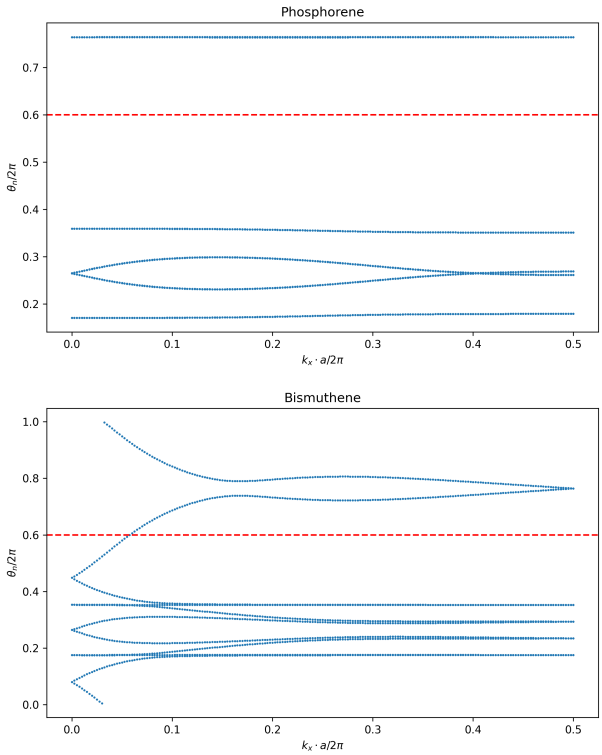

Figure 5: *Wilson loops computed by WannierTools [14] for phosphorene (top) and bismuthene (bottom). In red, an arbitrary reference line, in blue, the WCCs as a function of k_x. Our reference line is crossed an even number of times (zero times) by the WCCs of phosphorene. This means that phosphorene is a trivial insulator, with $\nu = 0$. The reference line is crossed an odd number of times (once) by the WCCs of bismuthene. This means that bismuthene is a topological insulator, with $\nu = 1$. The same would be true for any other reference line.*

The results of the Wilson loop calculations are shown in Fig. 5. We can see that phosphorene is a trivial insulator, with $\nu = 0$, while bismuthene is a topological insulator, with $\nu = 1$. This is consistent with the expectation that strong SOC can lead to topological non-triviality.

Nanoribbon Calculations

To investigate the edge states of phosphorene and bismuthene, we constructed 8 cell thick nanoribbons of both. The crystalline structure is taken from the bulk

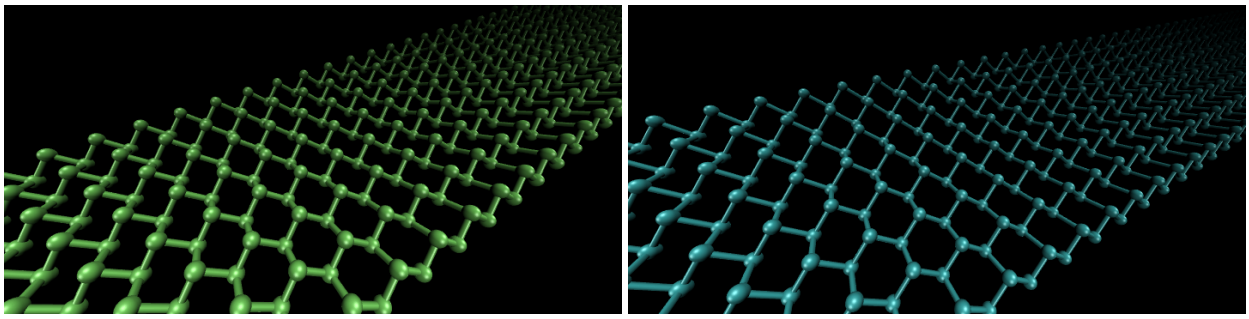

Figure 6: *Optimized structures of 8 cell thick nanoribbons of phosphorene (left) and bismuthene (right). Images obtained in VMD [7]. The two materials have the same hexagonal lattice, with different lattice constants and out-of-plane displacements of the atoms. The lattice constants are* $a^P = 3.281$ *Å and* $a^{Bi} = 4.350$ *Å. The out-of-plane displacements are* $\Delta z^P = 1.243$ *Å and* $\Delta z^{Bi} = 1.735$ *Å.*

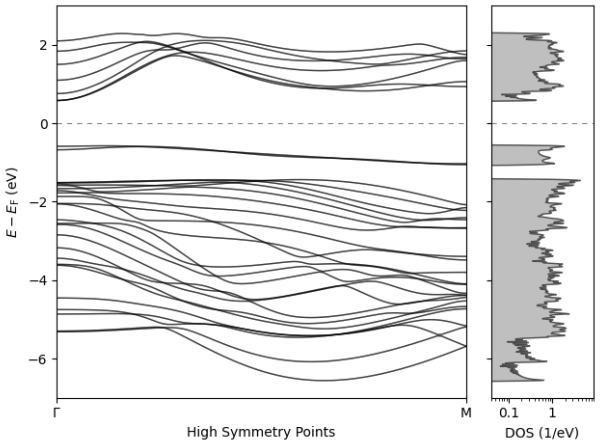

Figure 7: *Computed density of states (on the right) and band structure (on the left) for phosphorene nanoribbons of thickness 8 cells. The energies are given with respect to the Fermi energy, which lies in the middle of the gap. The gap is* $E_G^P = 1.1550\,\text{eV}$ *and the direct gap is* $E_{DG}^P = 1.1661\,\text{eV}$.

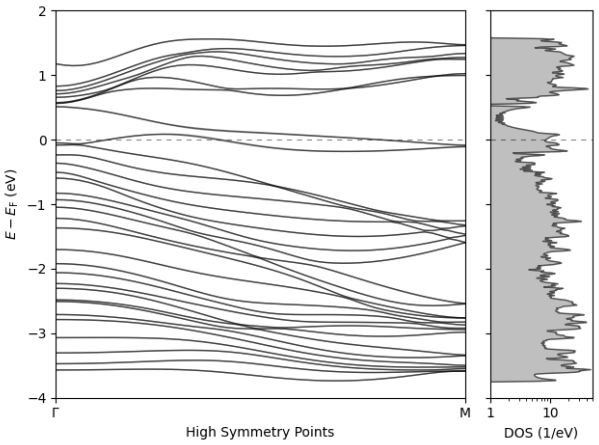

Figure 8: *Computed density of states (on the right) and band structure (on the left) for bismuthene nanoribbons of thickness 8 cells. The energies are given with respect to the Fermi energy, which crosses two (four, with spin degeneracy) bands that cross the bulk gap.*

relaxation done before, as relaxing these structures, with unit cells containing 16 atoms, would be too computationally expensive given that non-collinear spin calculations are very demanding. The structures are shown in Fig. 6.

All calculations[7] are done with non-collinear SOC and without constraints on magnetization. A vacuum of 4 times the lattice constant is added in the directions orthogonal to the nanoribbon to avoid interactions between periodic images.

The scf calculations are done with a $12 \times 1 \times 1$ Monkhorst-Pack k-point grid, a plane wave cutoff of 35 Ry and a density cutoff of 140 Ry. The nscf calculation is done with a $50 \times 1 \times 1$ Monkhorst-Pack k-point grid, a plane wave cutoff of 35 Ry and a density cutoff of 140 Ry. The scf energy convergence threshold is set to 10^{-8} Ry.

After a first scf calculation, we performed a more precise nscf calculation, the results of which were used to compute the density of states using `dos.x`. Given that in 1D the BZ is a segment, this calculation was used to compute the band structure as well, using `bands.x`. The results are shown in Figs. 7 and 8.

We can see that the phosphorene nanoribbon is still an insulator, with a gap of $E_{\text{G}}^{\text{P,nr}} = 1.1550\,\text{eV}$ and direct gap $E_{\text{G}}^{\text{P,nr}} = 1.1661\,\text{eV}$. On the other hand, the bismuthene nanoribbon has become metallic, with edge states crossing the Fermi level. This is consistent with the bulk-boundary correspondence, which states that a non-trivial topological invariant in the bulk implies the existence of gapless edge states at the boundary of the system.

To verify that these states are indeed edge states, we plotted the charge density[8] of the states at $E -$

[7] Input files are available at https://github.com/coscialeo/num_meth.git.

[8] The 2D charge density is obtained by integrating the 3D charge density obtained with `pp.x` over the z direction.

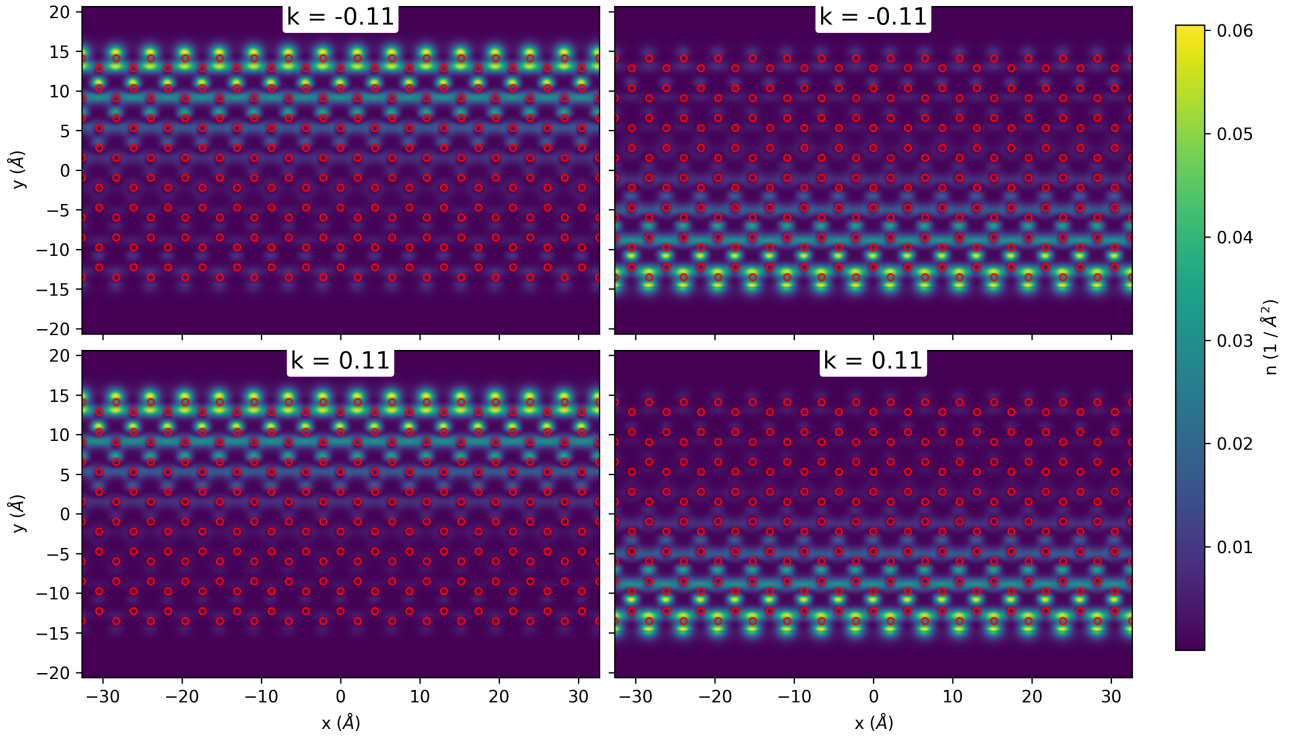

Figure 9: *Charge density of the states at $E - E_F = 0.308\,\text{eV}$ for bismuthene nanoribbons of thickness 8 cells. The atomic positions are shown as red circles. The two states at $k = \bar{k} = 0.11 \cdot 2\pi/a^{Bi}$ are shown on the top, while the two states at $k = -\bar{k}$ are shown on the bottom. We can see that two of them are localized at one edge, while the other two are localized at the opposite edge. In particular, each edge has a state at $k = \bar{k}$ and a state at $k = -\bar{k}$, which are therefore counterpropagating.*

$E_F = 0.308\,\text{eV}$[9] for bismuthene (see Fig. 9). The bands that cross this energy level inside the bulk gap are four, two at $k = \bar{k}$ and two at $k = -\bar{k}$.

We can see that two of them are localized at one edge, while the other two are localized at the opposite edge. In particular, each edge has a state at $k = \bar{k}$ and a state at $k = -\bar{k}$, which are therefore counterpropagating. The localization is not perfect, as the states have some weight in the bulk of the nanoribbon, but this is expected given that the nanoribbon is only 8 cells thick.

In Fig. 10 we plot the density of spin[10] along the out of plane direction, s_z, for two states on the same edge, one at $k = \bar{k}$ and one at $k = -\bar{k}$. We can see that the two states have opposite spin, confirming the helical nature of the edge states. This spin-momentum locking is a hallmark of topological insulators and is responsible for the suppression of backscattering from non-magnetic impurities.

[9] The Fermi level is crossed once by the upper bands in Fig. 8 and twice by the lower bands. This makes the picture needlessly complicated, so we opted for an energy level, still in the bulk gap, that is crossed only once.

[10] Obtained in the same way as the charge density.

Calculation Parameters

All pseudopotentials and input files for the Quantum ESPRESSO, Wannier90 and WannierTools calculations above can be found freely at https://github.com/coscialeo/num_meth.git.

Python was used for data analysis and plotting, using the NumPy and Matplotlib libraries. These scripts are not included in the repository.

References

[1] M. Z. Hasan and C. L. Kane. "Colloquium: Topological insulators". In: *Rev. Mod. Phys.* 82 (4 Nov. 2010), pp. 3045–3067. DOI: 10.1103/RevModPhys.82.3045.

[2] C. L. Kane and E. J. Mele. "Z_2 Topological Order and the Quantum Spin Hall Effect". In: *Phys. Rev. Lett.* 95 (14 Sept. 2005), p. 146802. DOI: 10.1103/PhysRevLett.95.146802.

[3] L. Fu and C. L. Kane. "Time reversal polarization and a Z_2 adiabatic spin pump". In: *Phys. Rev. B* 74 (19 Nov. 2006), p. 195312. DOI: 10.1103/PhysRevB.74.195312.

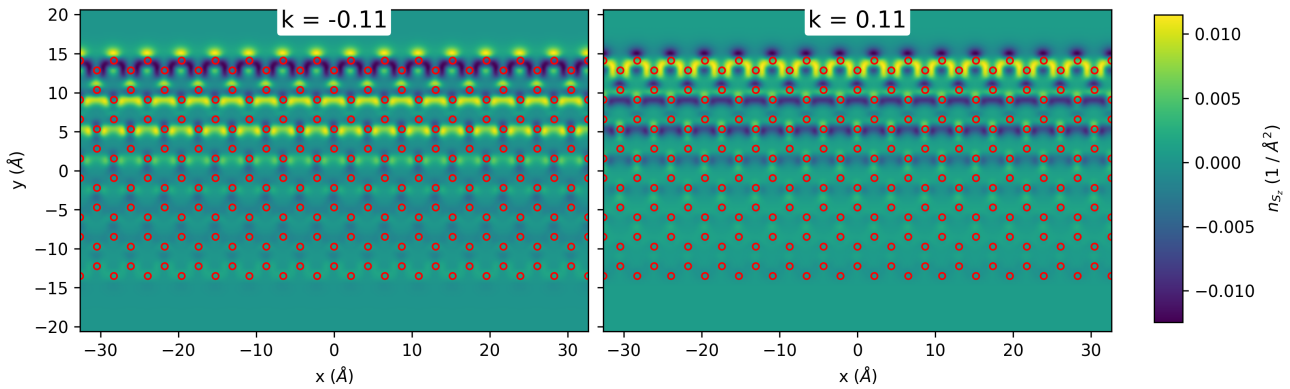

Figure 10: *Spin density of the two states at $E - E_F = 0.308\,\text{eV}$ localized at the same edge of bismuthene nanoribbons of thickness 8 cells. The atomic positions are shown as red circles. The state at $k = \bar{k} = 0.11 \cdot 2\pi/a^{Bi}$ is shown on the right, while the state at $k = -\bar{k}$ is shown on the left. We can see that the two states have opposite spin, confirming the helical nature of the edge states.*

[4] P. Giannozzi et al. "QUANTUM ESPRESSO: a modular and open-source software project for quantum simulations of materials". In: *Journal of Physics: Condensed Matter* 21.39 (Sept. 2009), p. 395502. ISSN: 1361-648X. DOI: 10.1088/0953-8984/21/39/395502.

[5] P. Giannozzi et al. "Advanced capabilities for materials modelling with Quantum ESPRESSO". In: *Journal of Physics: Condensed Matter* 29.46 (Oct. 2017), p. 465901. ISSN: 1361-648X. DOI: 10.1088/1361-648x/aa8f79.

[6] P. Hohenberg and W. Kohn. "Inhomogeneous Electron Gas". In: *Phys. Rev.* 136 (3B Nov. 1964), B864–B871. DOI: 10.1103/PhysRev.136.B864.

[7] W. Humphrey, A. Dalke, and K. Schulten. "VMD – Visual Molecular Dynamics". In: *Journal of Molecular Graphics* 14 (1996), pp. 33–38.

[8] W. Kohn and L. J. Sham. "Self-Consistent Equations Including Exchange and Correlation Effects". In: *Phys. Rev.* 140 (4A Nov. 1965), A1133–A1138. DOI: 10.1103/PhysRev.140.A1133.

[9] J. P. Perdew, K. Burke, and M. Ernzerhof. "Generalized Gradient Approximation Made Simple". In: *Phys. Rev. Lett.* 77 (18 Oct. 1996), pp. 3865–3868. DOI: 10.1103/PhysRevLett.77.3865.

[10] P. Scherpelz, M. Govoni, et al. "Implementation and Validation of Fully Relativistic GW Calculations: Spin–Orbit Coupling in Molecules, Nanocrystals, and Solids". In: *Journal of Chemical Theory and Computation* 12.8 (Aug. 2016), pp. 3523–3544. ISSN: 1549-9618. DOI: 10.1021/acs.jctc.6b00114.

[11] H. J. Monkhorst and J. D. Pack. "Special points for Brillouin-zone integrations". In: *Phys. Rev. B* 13 (12 June 1976), pp. 5188–5192. DOI: 10.1103/PhysRevB.13.5188.

[12] L. Talirz, S. Kumbhar, et al. "Materials Cloud, a platform for open computational science". In: *Scientific Data* 7.1 (Sept. 2020), p. 299. ISSN: 2052-4463. DOI: 10.1038/s41597-020-00637-5.

[13] N. Mounet, M. Gibertini, et al. "Two-dimensional materials from high-throughput computational exfoliation of experimentally known compounds". In: *Nature Nanotechnology* 13.3 (Mar. 2018), pp. 246–252. ISSN: 1748-3395. DOI: 10.1038/s41565-017-0035-5.

[14] Q. Wu, S. Zhang, et al. "WannierTools : An open-source software package for novel topological materials". In: *Computer Physics Communications* 224 (2018), pp. 405–416. ISSN: 0010-4655. DOI: https://doi.org/10.1016/j.cpc.2017.09.033.

[15] A. A. Mostofi, J. R. Yates, et al. "An updated version of wannier90: A tool for obtaining maximally-localised Wannier functions". In: *Computer Physics Communications* 185.8 (2014), pp. 2309–2310. ISSN: 0010-4655. DOI: https://doi.org/10.1016/j.cpc.2014.05.003.

[16] R. Yu, X. L. Qi, et al. "Equivalent expression of Z_2 topological invariant for band insulators using the non-Abelian Berry connection". In: *Physical Review B* 84.7 (Aug. 2011). ISSN: 1550-235X. DOI: 10.1103/physrevb.84.075119.